



# Geotechnical Zonation and $V_s^{30}$ Classification of Soil for Seismic Site Effects Evaluation in the Western Extension of New Aswan City, Egypt

AHMED M. MENEISY,<sup>1,4</sup> AHMED HAMED,<sup>2,3,5</sup> MOHAMED KHALIFA,<sup>2</sup> MOHAMED EL BOHOTY,<sup>2</sup> ESSAM GHAMRY,<sup>2</sup> and AYMAN TAHA<sup>2</sup>

**Abstract**—The Egyptian government has been constructing several new cities in recent years to accommodate the rapidly growing population. One of these cities is located in the western extension of New Aswan City. The primary goal of this study is to identify the dynamic engineering properties of underlying rocks by analysis of compressional and shear-wave velocities. Additionally, the  $V_s^{30}$  for site classification has been estimated to delineate the potential likely causes of structural building damages. Engineering features and several significant elastic moduli were assessed. The proposed site consists of two geoseismic units: the upper layer is composed of gravel, friable sands, and sandstone in some places, while the second layer is characterized by stiff sandstone with clay intercalations. They are low- to high-competence rock, respectively. By applying the NEHRP's guidelines,  $V_s^{30}$  was estimated for near-surface geologic units. Consequently, the defined site was split into two categories: type C, which describes the major part of the area, and class B (rigid rock). In addition, to evaluate the site effects, the soil amplification and site natural period have been estimated to avoid any probable impact of the interactions between the soil and structure. The soil conditions of the study area tend to form a possible danger for one to three story structures during any possible earthquake. In conclusion, the estimated geotechnical characteristics and site classification principally act as a key for seismic site evaluation, which will utilize as input parameters for civil construction purposes.

**Keywords:** New Aswan City,  $V_s^{30}$ , NEHRP, site effects, soil amplification, natural period.

## 1. Introduction

One of the numerous new cities being built in Egypt is New Aswan City. It was established in 1999 and built to address the issue of insufficient accommodations. The location under study is on the western riverbank of the Nile, between latitudes  $24^\circ 09' 20''$  and  $24^\circ 13' 07''$ N and longitudes  $32^\circ 50' 18''$  and  $32^\circ 52' 08''$ E. The recent study conducted the seismic survey for the non-studied extension of New Aswan City (Fig. 1). The aims of the current study are to apply shallow seismic refraction and MASW technique to estimate the compressional and shear wave velocities for geotechnical parameters estimation and  $V_s^{30}$  computation to determine site class and to estimate the soil amplification and site natural periods of the study area, according to the National Earthquake Hazards Reduction Program Provisions (NEHRP, 2003) and ECP-201 (2012), to avoid any probable soil-building interaction effects throughout the construction in the extension of New Aswan City.

The assessment of ground response is one of the most important and often encountered issues in geotechnical earthquake engineering. It is well known that any probable damage to buildings by earthquakes is significantly related to the subsoil conditions (Kanai, 1952; Ooba, 1957). Therefore, the obtained data on the regional soil conditions will be crucial for risk evaluation and establishing mitigation strategies. To assess the essential building characteristics and clarify issues regarding underlying rocks and soils, the shallow seismic refraction and Multi-Channel Analysis of Surface Wave (MASW) techniques are employed for geotechnical site investigation purpose (Park et al., 1999). Rayleigh

<sup>1</sup> Department of Geology, Faculty of Science, Aswan University, Aswan, Egypt.

<sup>2</sup> National Research Institute of Astronomy and Geophysics, Helwan, Egypt. E-mail: ahmadhamed4@nriag.sci.eg

<sup>3</sup> Aswan Regional Earthquake Research Center, Aswan, Egypt.

<sup>4</sup> Department of Earth Resources Engineering, Faculty of Engineering, Kyushu University, Fukuoka, Japan.

<sup>5</sup> Department of Mathematics and Geosciences, Trieste University, Trieste, Italy.

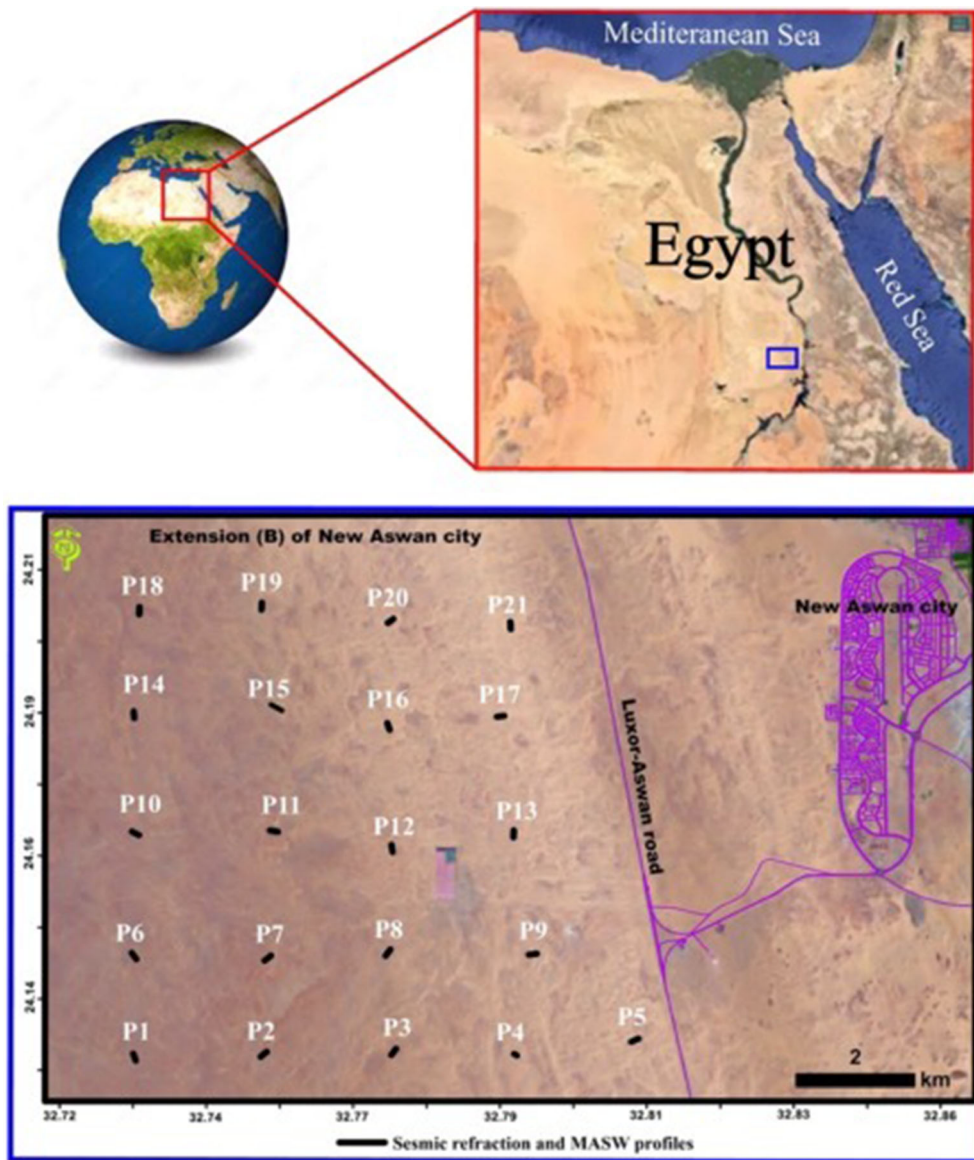


Figure 1  
Location of the study area with SSR and MASW profiles

wave analysis of seismic signal recordings yields shear wave values for the surface/subsurface soils (Miller et al., 1999; Mohammed et al., 2020; Xia et al., 2000). Practically, these geophysical methods may precisely identify a subsurface bedrock as well as lateral and vertical soil property variations (Whiteley, 1994).

There are various case studies where collaborative geophysical approaches have been used such as refraction, MASW, and ERT for geotechnical site evaluation (Abudeif et al., 2017; El-Moghazy, 2017; Fat-Helbary et al., 2019a, 2019b; Hamed, 2019; Mohammed et al., 2018) and landslide detection (Grit & Kanli, 2016) in addition to dam safety research

(Hodgkinson & Brown, 2005; Lankston, 1989; Yilmaz et al., 2006).

## 2. Overview of Geology and Earthquake Activity

Numerous authors have examined the overall geologic framework of the studied area and its environs, including Issawi et al., (2009a, b), El Bastawesy et al. (2010), and Yousif (2019). Outcropping Precambrian crystalline hard igneous and metamorphic rocks are predominant in the geology of the Aswan area, and these rocks are overlain by a Cretaceous Nubian Sandstone deposit (EGSMA, 2002).

Basement rocks and subsequent weathering products form the bottom of the stratigraphic succession. Most of these are covered by sandstone formations. The Aswan area has a sandstone sequence that is anywhere from 70 to 162 m thick. Based on the existence of oolitic iron ore deposits, it has been classified into three distinct layers (Attia, 1955; Youssef, 2003). The Abu Aggag Formation, dating back to the Turonian period, is the oldest depositional layer and is composed of coarse sandstone with mudstone interbeds. The Timsah Formation consists of siltstone, sandstone, shales, and an iron ore deposit; it dates to the Coniacian to Santonian periods and is situated above the Abu Aggag Formation. The Um Barmil Formation, made up of moderate-sized sandstone with claystone intercalations and dating back to the Campanian period, lies northeast of the research area. The Nubian Sandstone is covered by Quaternary sediments, including Darb El Gallaba gravel, conglomerates, playa, alluvium-eluvium, and surficial sediments that are primarily alluvium (Fig. 2).

Fat-Helbary et al. (2006) used geophysical and geotechnical data to study the initial section of New Aswan City located directly along the riverbank. They concluded that there are two to three underlying layers in the studied region; the first layer is fine sand intercalated with fragments of clay. The second stratum is mostly formed of fragments of fracture of sandstone intercalated with gravel. Finally, the third layer is composed mainly of sandstone. In addition, the structural trend analysis technique for the acquired magnetic data is utilized to determine the

location of the tectonic lines for the area. The results indicate that there are two major faults more or less in the N–S to NW–SE directions, in addition to minor faults with various trends (Fat-Helbary et al., 2004).

Regional basement rock uplift and regional faulting govern the structural layout of the Aswan region (Issawi, 1968). In the Aswan highlands, Precambrian basement granite has been exposed as a consequence of the structural high that has developed east of the Nile Valley. The Nubia Formation and underlying stratigraphic units have been gradually tilted toward the west and northwest. These units often experience regional dips of  $1^\circ$  to  $2^\circ$  (WCC, 1985). Local faults are overlaid on the largely horizontally structure of the Nubian Plain, Sinn El-Kaddab Plateau, and Aswan Hills to the east of Lake Nasser. The region of Lake Nasser, which hosts multiple notable faults inside the Western Desert fault networks, was divided into several categories according to the faults' patterns. The east-west trend (Kalabsha and Seiyal fault) and north-south trend (Khor El Ramla, Kurkur, Gebel El-Barqa, Gazelle, and Abu Dirwa fault) are the two most significant faults among them. The spillway fault is one of several dispersed faults (El Bohoty et al., 2023) found in the region (Fig. 3).

The earthquake coverage of the Upper Egypt region grew more consistent with the beginning of worldwide seismograph operation and data analysis in 1900, but it is still at the threshold value of magnitude 4.5 attributed mostly to the distance from seismic stations. Seismographs at Aswan and Abu Simbel were added by the Helwan Observatory in 1975, enabling identification of the epicenters of the seismic events that were too minor to be felt. After the earthquake of November 14, 1981, a radio-telemetry network of 13 stations was set up to monitor micro-seismic events in the northern half of the Nasser Lake. According to Simpson et al. (1986), the earthquake activity in and around the Kalabsha fault is centered on two separate clusters in the Aswan region. Several scientists and researchers have studied the Aswan area's seismic activity (e.g., El-Khashab et al., 1991; Kebeasy et al., 1987; Simpson et al., 1986). The seismic activity map surrounding the study region is constructed using the new earthquake data catalog for the years 1981–2021 (Fig. 4).

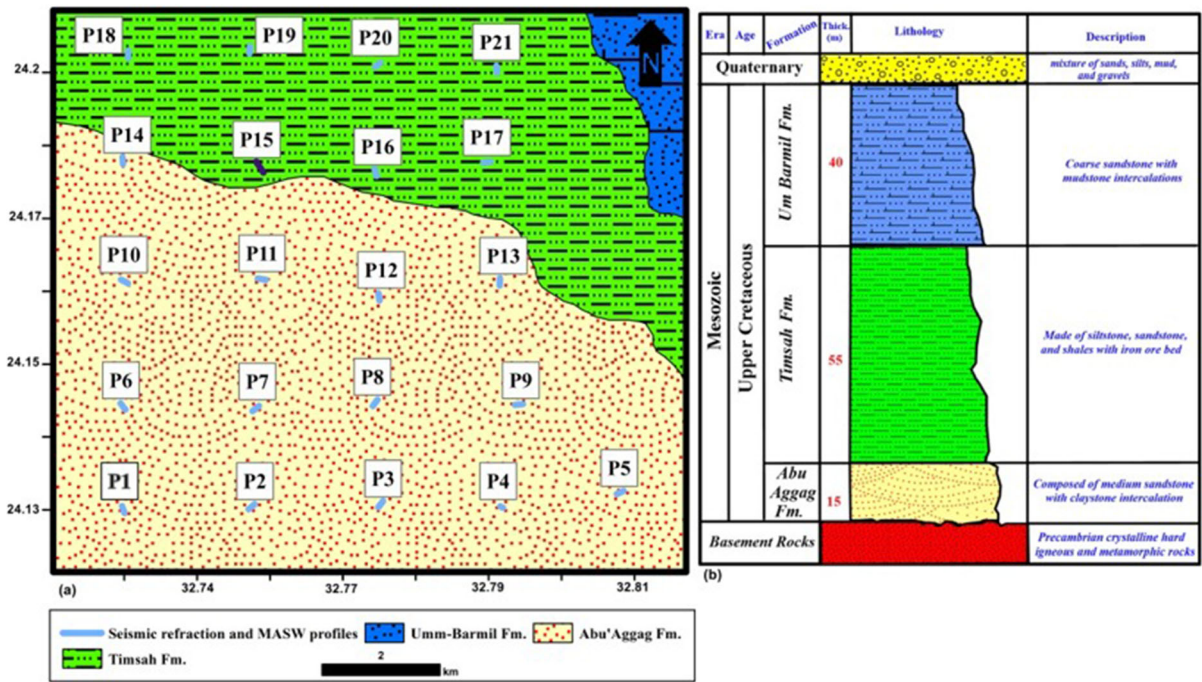


Figure 2 Geologic map of study area (a); the main geologic cross-section shows the lithologic succession (b) (after EGSMA, 2002)

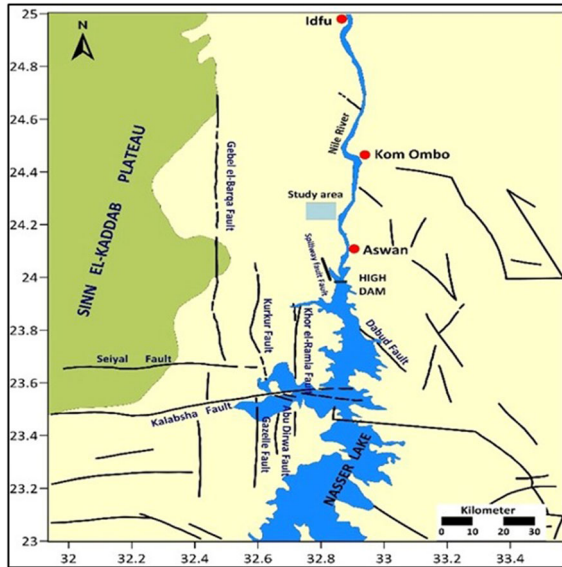


Figure 3 Active and inactive fault system map of the study area (after Conoco, 1987)

The catalog’s analysis reveals that seismic activity is localized at the point where the N–S and E–W fault

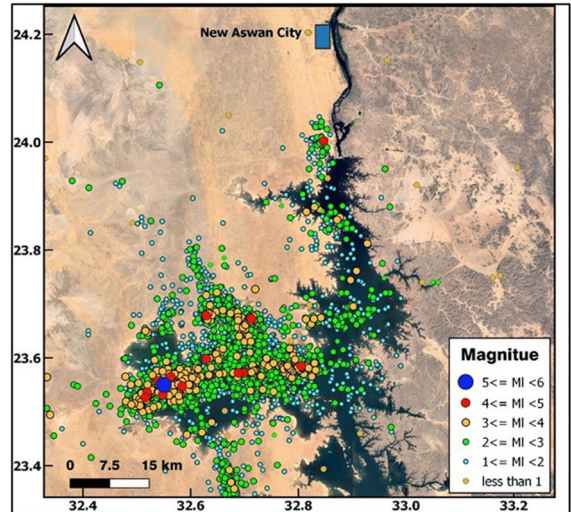


Figure 4 Seismicity map of the study area for 1981–2021

networks intersect. The spillway fault region, contrarily, is near the research area and has experienced a significant rise in microearthquake activity (El-Bohoty et al., 2023). The yearly rise in lake water level, which exceeded 180 m and reached its highest

level (181.6 m) in 1999, has been ascribed to the abrupt increase in seismicity in the spillway region from 1999 to 2002. After the lake's water level reached 180.11 m in October 2007, the earthquake of 2010 and its aftershocks occurred.

### 3. Geophysical Measurements

By establishing an acquisition mechanism for forwarding, mid-point, and reverse P-wave shoots (Hamed, 2019; Hamed et al., 2023; Fat-Helbary et al., 2019b), as well as a forward system for surface wave shootings, 21 profiles for both shallow seismic refraction and MASW techniques were established to calculate the  $V_p$  and  $V_s$  of the subsurface soil in the region. Each measured location has two types of profiles. These profiles were oriented according to the topography of each site.

In this study, the shallow seismic refraction (SSR) data were collected utilizing a 48-channel signal geometrics seismograph; therefore, seismic waves were generated using a 15-kg sledgehammer and recorded by vertical geophones (40 Hz), which had to be used and firmly fastened to the ground for good ground coupling (Fat-Helbary et al., 2019b; Luna & Jado, 2000; Mohammed et al., 2020). All of the profiles were constructed with 115 m length with 5-m geophone spacings. Three shots were carried out: two at the terminals of each profile and the third one in the midpoint (Fig. 5). The sample interval and total recording length were 0.25 ms and 0.75 s, respectively.

Using the 1D MASW approach, S-waves were produced (Park et al., 1999, Abbas et al., 2023). Hence, MASW profiles were performed along the same profiles of seismic refraction lines (P-wave). Consequently, the surface wave survey was done using a low-frequency (4.5 Hz) vertical geophone (Stokoe et al., 1994), utilizing a seismic array with length of 46 m and 2 m offset distance. It was suggested to use a 15-kg sledgehammer to create seismic energy for active source surface wave studies. To prevent near- and far-field effects, two shoots were conducted at distances of 5 and 10 m before the first geophone with vertical stacking from three to five shoots to considerably reduce ambient noise (Fig. 6). Consequently, a 1-ms sampling interval with a 2-s total recording length ( $T = 2$  s) is the most typical parameter adopted here.

### 4. Data Processing

To analyze the obtained refraction data (forward, middle, and reverse) (Fig. 7a), the SeisImager/2D software package (2019) is utilized. As seen in Fig. 7b, the travel-time curves are produced by considering the survey line's length, space between receivers (geophones), source position, and initial arrival time (Veezhinathan & Wagner, 1990). Travel-time curves are corrected and checked to provide an accurate approximation of the P-wave velocity structure (Sheehan et al., 2005). The ultimate depth-velocity models are represented in two dimensions (Fig. 7c). Depending on the numbers of layers, which rely on how much the slope of the travel-time curve

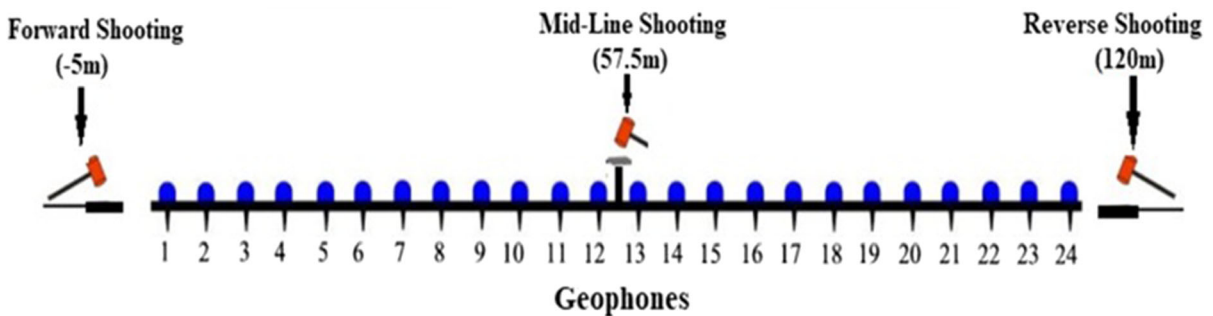


Figure 5  
Refraction survey with shot location and geophone spreading

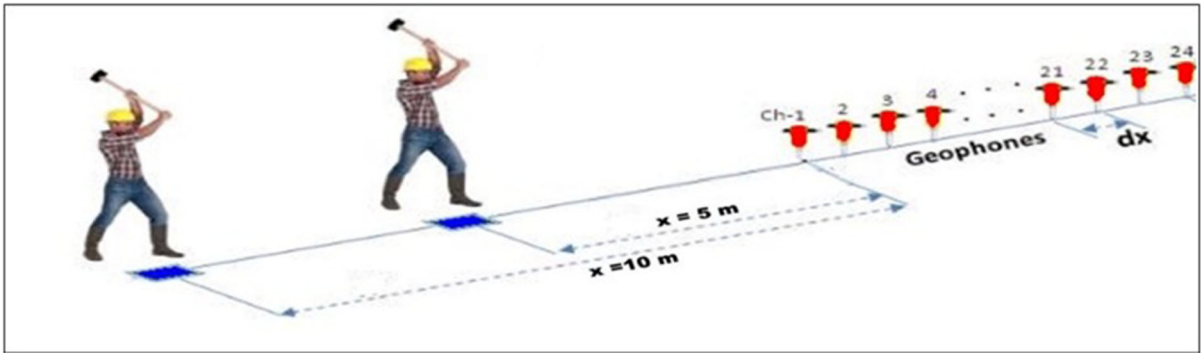


Figure 6  
Active MASW data acquisition field setup for generating 1D-Vs model

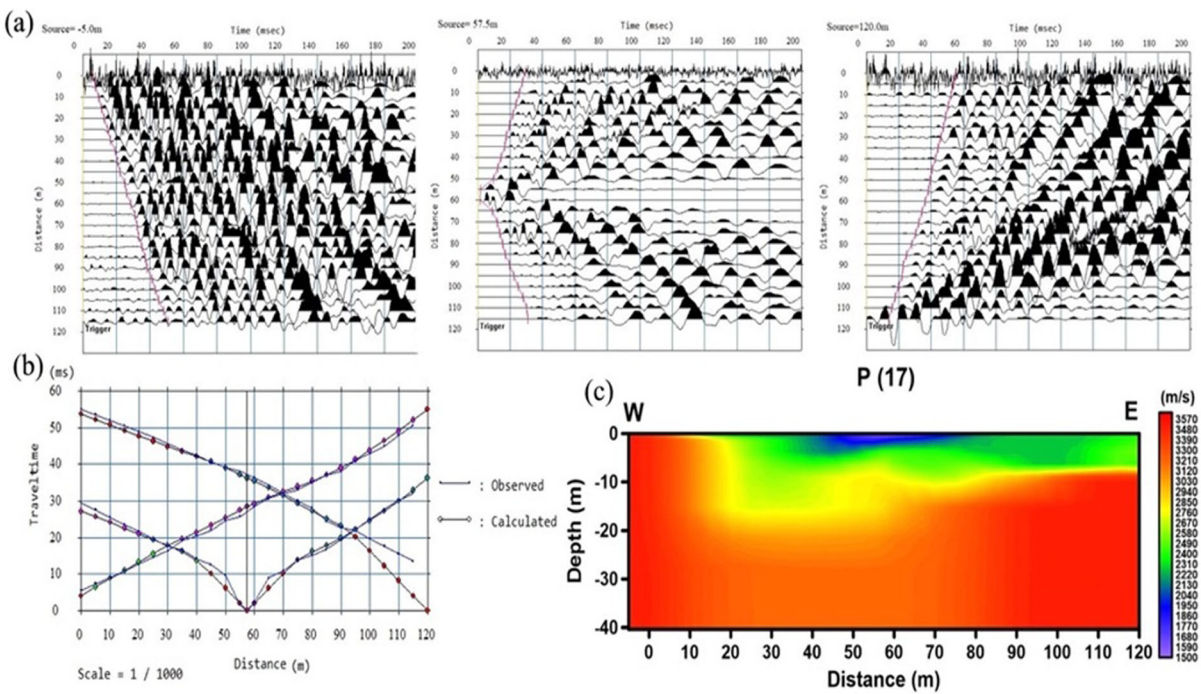


Figure 7  
Steps of shallow seismic refraction processing **a** forward, middle, and reverse shootings; **b** travel-time curve, and **c** 2D velocity model

varies (Ellefsen, 2009), two- or three-layered models have been implemented in the processing. The travel-time dispersion curve, on the other hand, clearly indicates a slight change and reveals three layers. The third layer has a slightly different velocity value and has been regarded as a transition zone between the over- and overlaid strata. Due to its small thickness, it is simply considered as two layers (Fig. 7c).

To compute the 1D-MASW velocity model, SeisImager/SW software (SeisImager, 2009; Underwood, 2007) was utilized. The MASW data processing passed through converting of the recorded signals from time domain (Fig. 8a) to frequency domain (Fig. 8b), followed by creating dispersion curves (Fig. 8c). The frequency range of 5–42 Hz has been selected for the frequency-phase velocity image.

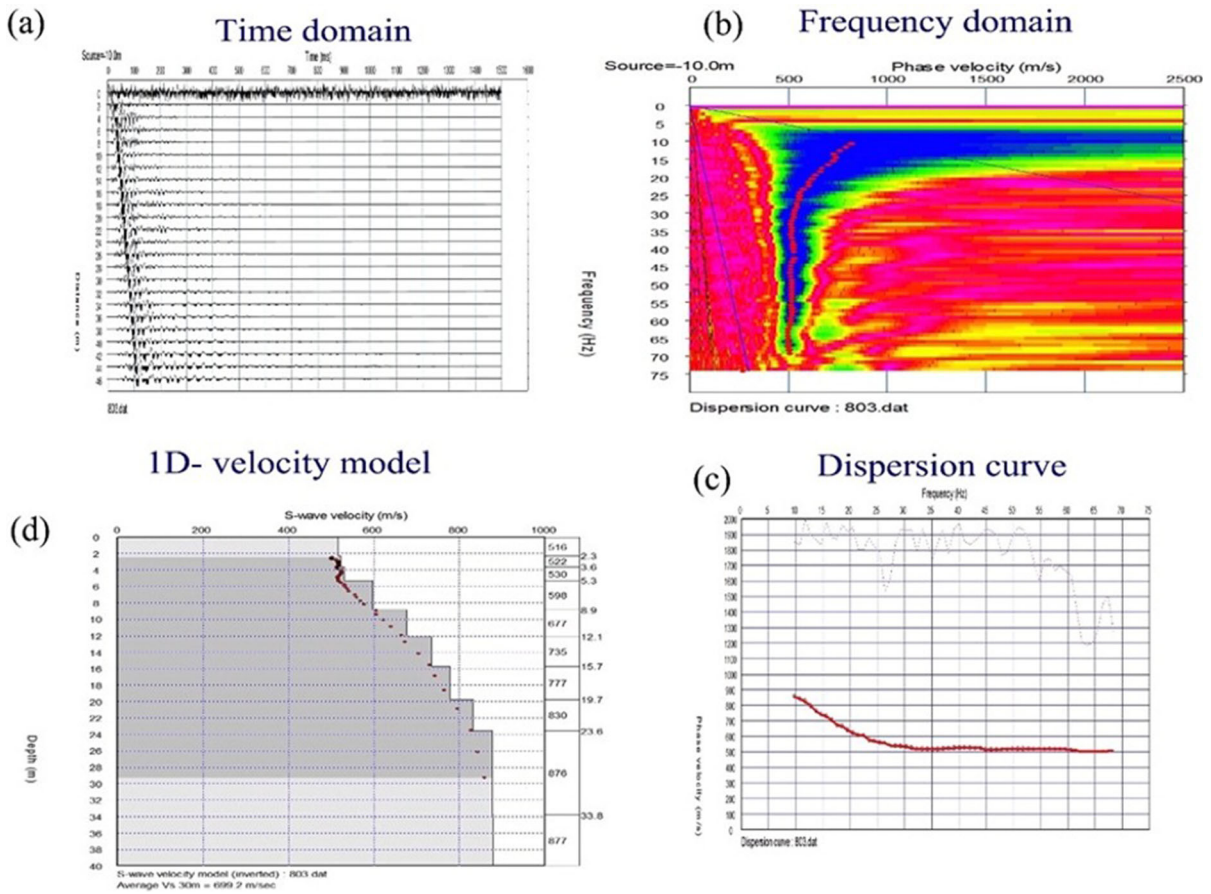


Figure 8 Procedure of MASW data processing using SeisImager software (ex. Profile No. 8)

Finally, a profile of the shear wave velocity has been generated (Fig. 8d).

### 5. Results and Data Interpretation

The description of seismic refraction records is often applied to compute the correct velocities for each investigation layer as well as to determine the depth under the shot point and each geophone. The interpretation of the data is based on an iterative ray-tracing approach, and the final 2D velocity-depth models for subsurface in form of  $V_p$  were generated (Fig. 7e). For the same site, S-wave dispersion curves and corresponding shear wave 1D-velocity models have also been constructed (Fig. 8). The ultimate

seismic velocities of many strata were calculated for each observed location.

Typically, we chose a two-layered model because of two considerations. The very little variations in seismic velocities caused us to define it as two different strata. The second hypothesis is that, in accordance with the geologic map and lithological cross-section shown in Fig. 2, the measured points are located in either the Abu Aggag Formation or Timsah Formation, both of which often have a few meters of Quaternary deposits on the top. In addition, the rocks exposed in the work area support our explanation.

Therefore, two layers in the seismic cross-sections of subsurface strata are produced. According to the distinct variation in shear wave velocities, a surface layer made up of friable sand and gravel particles

constitutes the first geoseismic zone, which ranges in thickness between 0.5 and 5 m, with P-wave velocities from 927 and 1900 m/s and shear wave velocities ( $V_s$ ) between 260 and 630 m/s. The second geoseismic layer has maximum seismic wave velocities ( $V_p$ ), which vary from 2000 to 3300 m/s and  $V_s$  from 520 to 1150 m/s, and comprises intercalations of sandstone with shale and clay. The results of  $V_p$ ,  $V_s$ , and the corresponding geotechnical parameters calculated for all investigated profiles are summarized in Figs. 9, 10, and 11 and Table 5.

### 5.1. Elastic and Geotechnical Parameters

The geotechnical site characteristics are crucial in the calculations of intensity distribution since rock sites regularly provide lower ground-motion intensities than less stiff areas (Dutta, 1984). A limited number of geotechnical criteria were chosen to assess whether subsurface materials were suitable for construction or not. In the current study, the calculated  $V_p$  and  $V_s$  were utilized to assess the elastic and geotechnical characteristics. Tables 1 and 5 provide an overview of the empirical equations of elastic, geotechnical, and petrophysical parameters used in

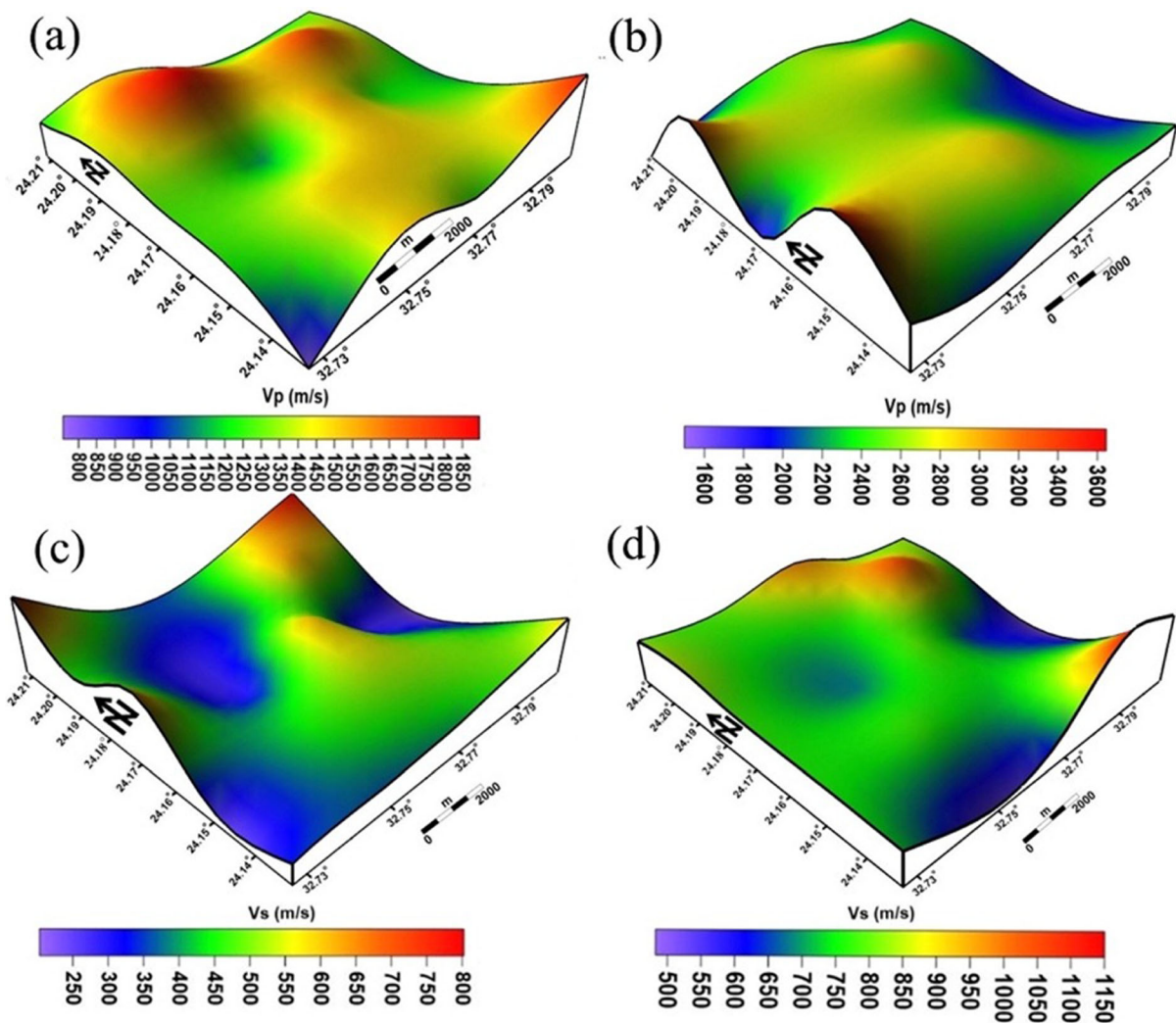


Figure 9

P and S seismic wave velocity distribution for the first (a, c) and second (b, d) geoseismic layers along the study area



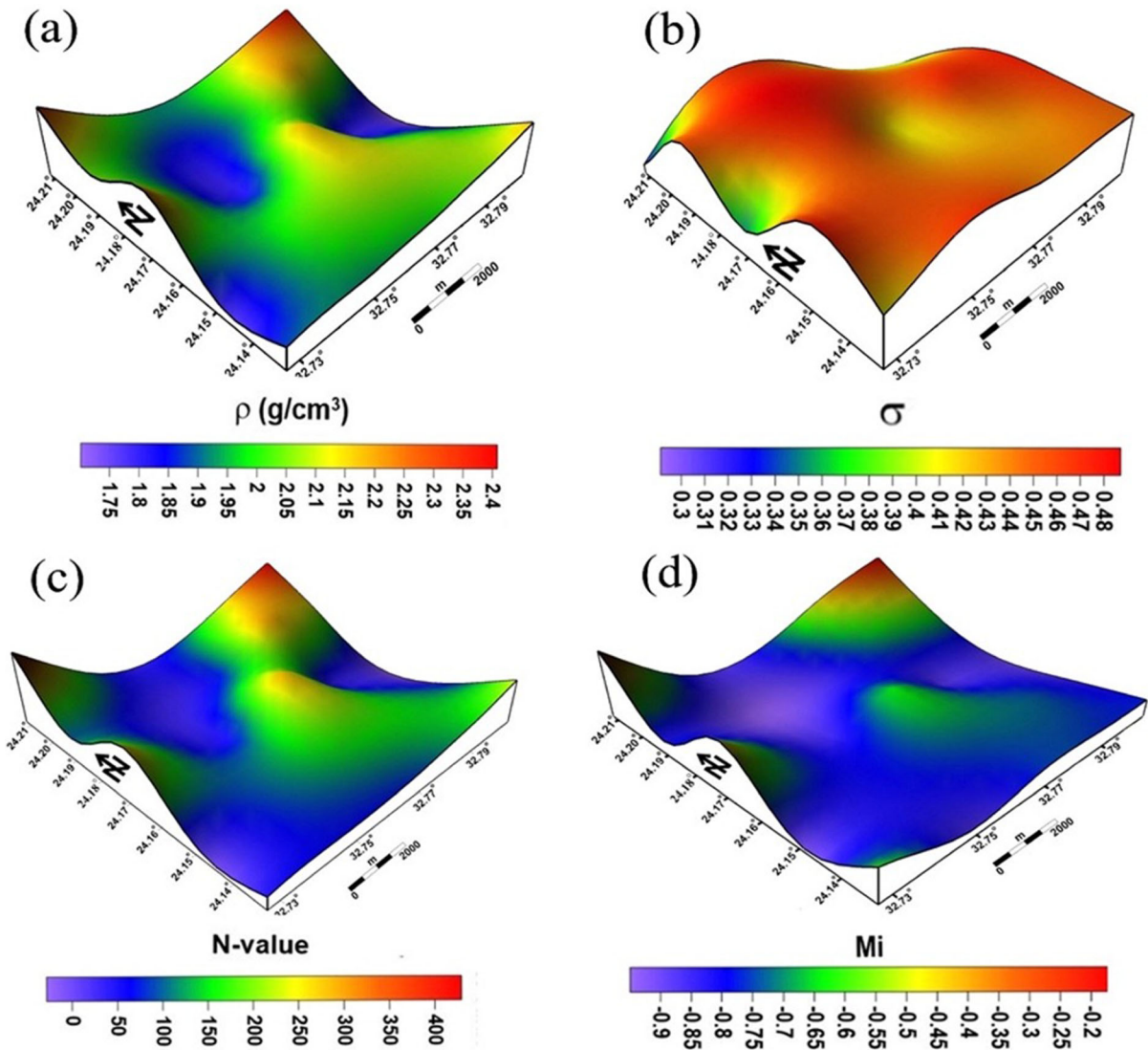


Figure 10

Selected elastic and geotechnical parameters for the surface layer: **a** density, **b** Poisson's ratio, **c**  $N$ -value, **d** material index

the current study in addition to the estimated values of those parameters. Currently, four geotechnical parameters have been selected to be discussed briefly here.

Density is one of the essential parameters that demonstrates how density causes the P-wave velocity to rise (Gardner et al., 1974). According to Keceli (2009), density values for the first and second layers range from 1.8 to 2.2 and 2.1 to 2.6  $\text{g/cm}^3$ , respectively (Figs. 10a, 11a). The second layer is distinguished by considerably large values; this

significant increase in calculated values is indicative of a rather high competent rock composition that characterizes the second stratum.

Furthermore, referring to the equation of Telford et al. (1976) and Kearey et al. (2002), Poisson's ratio ( $\nu$ ) shows the relative expansion strain to the relative compression strain under the given load (De Beer & Maina, 2008). Telford et al. (1976) classified the value as being 0.5 for fluids or friable sediments and approaching zero for tough rocks, typically zero for hard rocks, 0.25 for hard soil, and 0.5 for loose soil

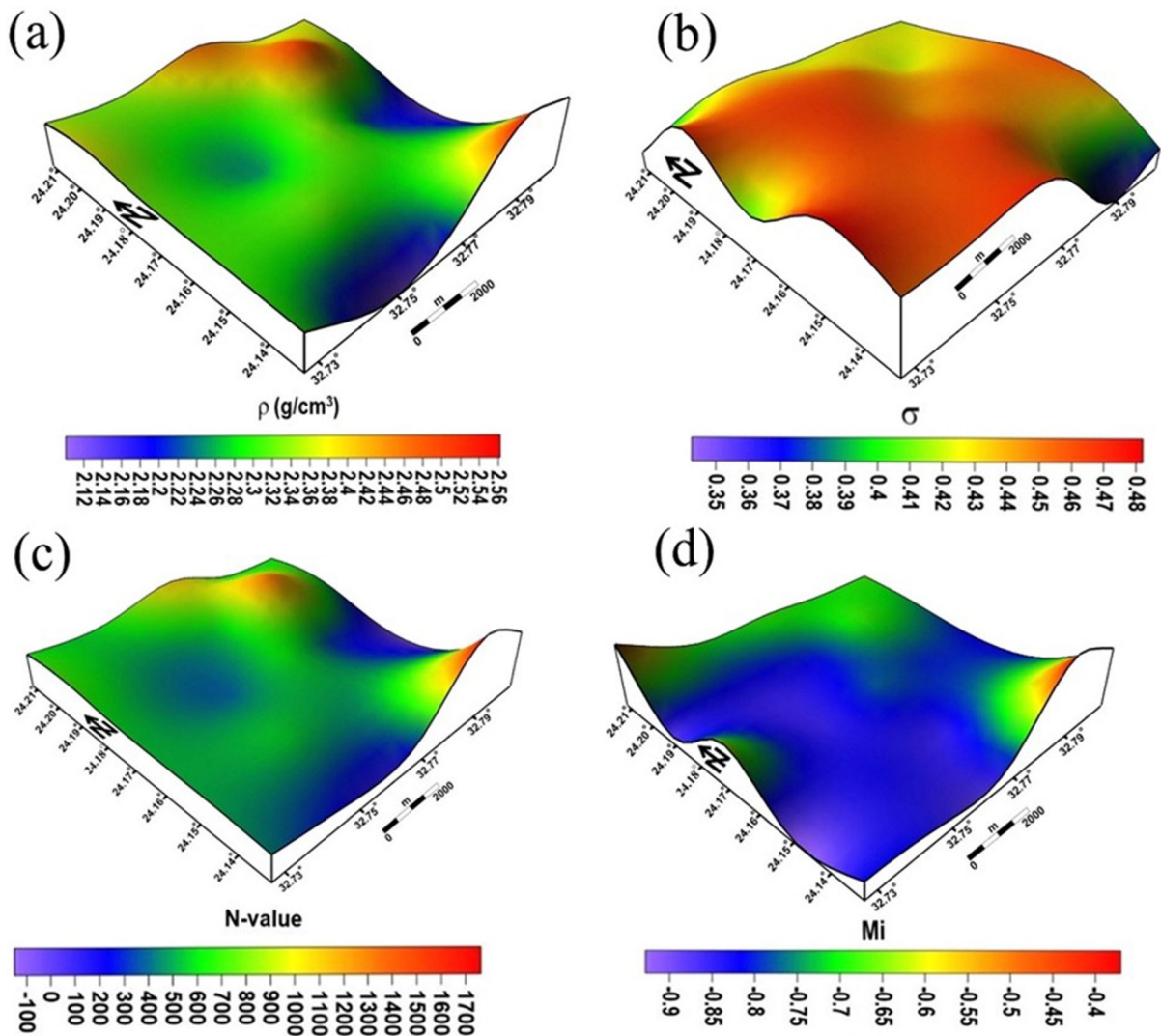


Figure 11

Selected elastic and geotechnical parameters for the second layer: **a** density, **b** Poisson's ratio, **c**  $N$ -value, **d** material index

(Table 2). This parameter's values in this study area are close to each other for the first and second layers (Figs. 10b, 11b). As a result, the sediments in the first and second strata range from being incompetent to significantly competent.

On the other hand,  $N$ -value according to Table 3 is a parameter used in geophysical evaluation to describe the material resistance to penetration by normalized cylindrical pointed bars under a load effect (Stümpel et al., 1984). Hence, the values fluctuated between 22.52 and 301.79 for the first layer (Fig. 10c) and between 171.92 and 1762.59 for the

second layer (Fig. 11c), both of which are made up of extremely thick and very dense materials (Bowles, 1984).

Material index ( $M_i$ ) is one of the geotechnical parameters that relates to the content of the entire material, the amount of consolidation, and whether or not fluids are contained inside the pore spaces, all of which have an impact on the wave velocities as a result of the medium of the materials (Abd El-Rahman, 1989). According to Sheriff and Geldart (1995), the derived material index values were divided into four major groups for foundational

Table 1

*Definition of elastic and geotechnical parameters used in this work*

Parameter	Equation used	References
Density ( $\rho$ )	$\rho = 0.44 V_s^{0.25}$	Keceli (2009)
Poisson's ratio ( $\sigma$ )	$\sigma = ((V_p/V_s)^2 - 2)/(2(V_p/V_s)^2 - 2)$	Telford et al. (1976), Kearey et al. (2002)
Rigidity modulus ( $\mu$ )	$\mu = \rho V_s^2$	Sharma (1978), Kearey et al. (2002)
Material index (Mi)	$M_i = (1 - 4\sigma)$	Abd El-Rahman (1989)
N-value	$V_s = 89.9N^{0.341}$	Stümpel et al. (1984), Imai and Yoshimura (1975)
Ultimate bearing capacity ( $Q_{ult}$ )	$\text{Log}Q_{ult} = 2.932(\text{Log}V_s - 1.45)$	Abd El Rahman et al. (1992)
Allowable bearing capacity ( $Q_a$ )	$Q_a = Q_{ult}/F$	Parry (1977)

Table 2

*Description of soil according to Poisson's ratio and material index (Birch, 1966; Mohammed et al., 2020; Sheriff & Geldart, 1995; Tatham, 1982)*

Soil description parameter	Incompetent to slightly competent	Fairly to moderately competent	Competent material	Very high competent material
Poisson's ratio	0.41 to 0.49	0.35 to 0.27	0.25 to 0.16	0.12 to 0.03
Material index	- 1 to - 0.5	- 0.5 to 0.0	0.0 to 0.5	> 0.5

considerations. The two layers' values fall within the group (I) of incompetent to moderately competent soils (Figs. 10d, 11d), which mostly refers to soft to competent deposits for the first and second layers, respectively.

## 5.2. $V_s^{30}$ and Site Classification

The microzonation map of any city must be created in accordance with the soil characteristics of that city to construct the optimal master plan. All technical challenges in building originate from disturbances of ground motion, which are controlled by subsurface geology. Therefore, knowledge of near-surface soil parameters, such as their elastic properties and how they affect the propagated seismic wave,

is essential for engineering and environmental applications (Mohammed et al., 2020).

Multichannel analysis of surface waves (MASW), which calculates shear wave velocities at shallow depths, is widely used because it makes determining the parameters much simpler and less expensive (Park et al., 1998). Therefore, in the current study, the  $V_s^{30}$  is suggested for examining the amplification factor and site effects on seismic waves propagating in the upper 30 m following data processing, as demonstrated in the previous section. Different velocity distribution maps were created at six different depths, 5, 10, 15, 20, 25, and 30 m, respectively, to determine the mean shear wave velocity variation with depth (Fig. 12). The top 5 m of soil's average velocity distribution (the effective thickness close to structure basements) is crucial, and in some instances,

Table 3

*Relationship between both N-values and type of soil (Bowles, 1984)*

Cohesionless soils	N-values	0–10	11–13	13–50	< 50
	State	Loose	Medium	Dense	Very dense
Cohesive soils	N-values	> 4	4–6	7–15	< 25
	State	Very soft	Soft	Medium	Hard

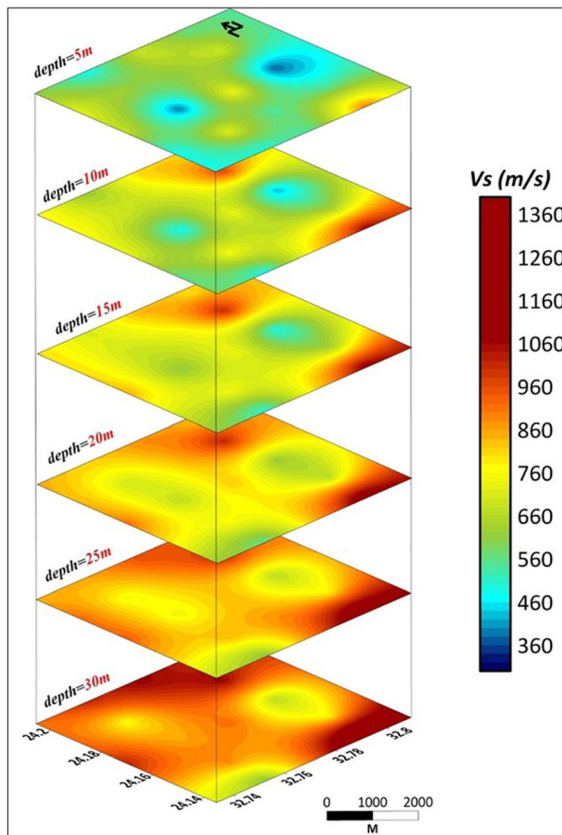


Figure 12

Average shear wave velocity distribution maps of the study area down to 5, 10, 15, 20, 25, and 30 m depth, respectively

a direct association may be observed between such a high amount of probable damage and low velocity. Two significant zones in the research region’s center have low  $V_s$  values of around 360 m/s, but when we descend into deeper strata, the value rises to > 760 m/s in the majority of the area, indicating the presence of highly compacted rocks.

Borcherdt (1994) first proposed a site classification depending on  $V_s^{30}$  parameter, which represents travel times from the ground’s surface to the topmost 30 m of depth. Subsequently, numerous contemporary seismic codes, including NEHRP, UBC97, IBC2000, and Eurocode8, were developed, using  $V_s^{30}$  to characterize the site (Dobry et al., 2000; Kanli et al., 2006). NEHRP site classification has been adopted in this study (Table 4).  $V_s^{30}$  is calculated using the following equation (CEN, 2004).

Table 4

Site classification using NEHRP (2003)

Site class	Description	Average shear wave velocity (m/s) top 30 m
A	Hard rock	$V_s(\text{avg})-30 > 1500$
B	Rock	$760 < V_s(\text{avg})-30 \leq 1500$
C	Very dense soil	$360 < V_s(\text{avg})-30 \leq 760$
D	Stiff soil	$180 \leq V_s(\text{avg})-30 \leq 360$
E	Soft soil	$V_s(\text{avg})-30 < 180$
F	Soils requiring site-specific evaluation	–

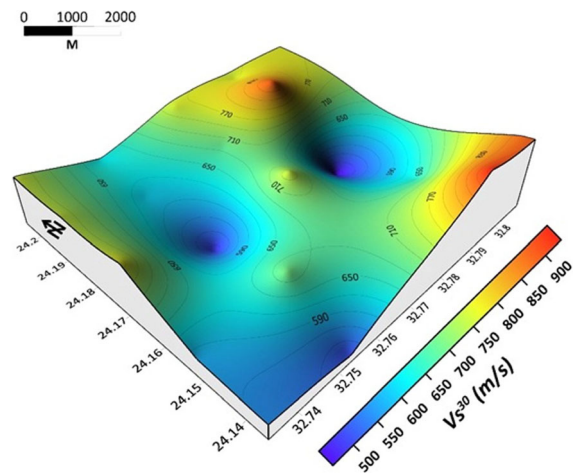


Figure 13

$V_s^{30}$  of the study area based on MASW measurement

$$V_s^{30} = \frac{30}{\sum_{i=1}^N \frac{h_i}{V_i}}$$

where  $V_i$  and  $h_i$  represent the thickness (m) and the  $V_s$  of  $i$ th layer, in a total of  $N$ , present in the upper 30 m.

The  $V_s^{30}$  values typically range from 450.8 to 935.4 m/s (Fig. 13); depending on NEHRP guidelines, the region is divided into two classes: class B (Rock) sites are found at the NE, SE, and middle portions of the studied area’s western edge, while Class C, which comprises the majority of the interested region, is characterized by very thick soil and soft rock (Fig. 14).

The  $V_s^{30}$  values of the Dinar area in Turkey are compared to the  $V_s^{30}$  values presented here based on the soil thickness of New Aswan City, Egypt.

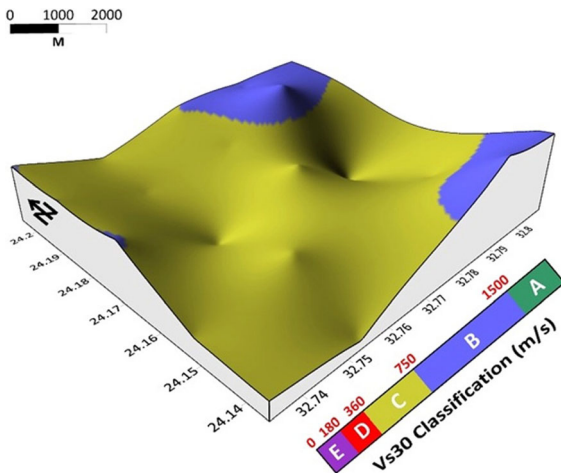


Figure 14

Site classification map of the study area based on NEHRP classification

According to El Bastawesy et al. (2010) and Yousif (2019), New Aswan City is situated on compacted sandstone, shale, and siltstone covered with shallow Quaternary deposits. In certain locations on the surface, compacted sandstone is visible. The estimated  $V_s^{30}$  values range from 450 to 935 m/s according on the soil thickness. The Turkish town of Dinar is situated on a tiny alluvial basin. The Quaternary soft soils throughout the basin's center are over 30 m thick (Kanli et al., 2008). The calculated  $V_s^{30}$  ranges from 160 to 240 m/s in the basin's middle region (Kanli et al., 2006). It is observed that the  $V_s^{30}$  values of both areas are different because of geologic condition (soil compaction and Quaternary deposit thickness) variation in both areas (Kanli 2010) (Table 5).

### 5.3. Soil Amplification and Site Natural Period

The estimation of site amplification values utilizing  $V_s^{30}$  has been shown to be one of the easiest methods for primarily estimating the amplification factor of seismic ground motion (Dobry et al., 2000; Kanli et al., 2006). Soft soils contribute significantly to earthquake damage and boost the intensity of the shaking that occurs during an earthquake. The shear wave velocity is a well-known index characteristic used to assess soil properties (e.g., soil amplification). Consequently, the  $V_s$  data acquired by the MASW

technique are employed in the current work to primarily and simply estimate the soil amplification of the site soil in the western extension of New Aswan City. The following equations provide the  $V_s^{30}$  and soil amplification ( $A$ ) relationships (Mid-ori-kawa, 1987):

$$A = 68V_s^{-0.6} (V_s < 1100 \text{ m/s})$$

$$A = 1 (V_s > 1100 \text{ m/s})$$

The soil amplification map, shown in Fig. 15, displays a qualitative evaluation of the soil's sensitivity to amplification. The resulting soil amplification value varied from 1.1 to 1.7, with high amplification in two central zones and at the southwest regions, where the layers were primarily loose deposits from the alluvial plain (Table 6).

Therefore, places with soft sediments in the soil, such as loose sands, silty clay, and gravels, are much more vulnerable to amplification. Lower shear wave velocities near 400 m/s are correlated with the outcrop of poorly consolidated Quaternary sediments in the work area when the amplification susceptibility map and  $V_s^{30}$  results are combined. Additionally, regions that are thought to be more prone to soil amplification based on the overlay approach correspond with areas of calculated lower shear wave velocities ( $V_s^{30} \leq 440 \text{ m/s}$ ).

The fundamental site period ( $T_s$ ) constitutes one of the significant indications for seismic hazard assessment, which is used to represent the initial phase of vibrating in soils. The following equation is used to compute it, which is determined by the thickness and  $V_s$  of the underlying soil (Kramer, 1995).

$$T_s = \frac{4H}{V_s}$$

where  $V_s$  is the average shear wave velocity of the overburden soil, and  $H$  is the overall thickness of the alluvium deposits. In the current study the depth ( $H$ ) in the equation above is set to 30 m, since the depth of 30 m below the surface is crucial for the construction of building foundations and is vulnerable to amplification of seismic ground motion (Boore, 2003; Boore et al., 2011). In addition, this assumption was obtained by Kramer's suggested quarter wavelength approximation (1995).

Table 5  
Elastic, geotechnical parameters,  $V_s^{30}$  values, and site classification at the study area

P. N	Layers no	$V_p$ (m/s)	$V_s$ (m/s)	$\rho$	$\sigma$	$\mu$	Mi	$N$ -value	Qult	Qa	$V_s^{30}$ (m/s)	Class
1	1	927	350	1.90	0.42	233,134	- 0.67	53.84	6.66	2.22	554.9	C
	2	2327	680	2.25	0.45	1,038,957	- 0.81	377.55	15.28	5.09		
2	1	1500	365	1.92	0.47	256,219	- 0.87	60.89	7.02	2.34	502	C
	2	2000	520	2.10	0.46	568,146	- 0.85	171.92	10.93	3.64		
3	1	1250	410	1.98	0.44	332,825	- 0.76	85.63	8.12	2.71	714.4	C
	2	2300	700	2.26	0.45	1,108,979	- 0.80	411.05	15.84	5.28		
4	1	1550	500	2.08	0.44	520,158	- 0.77	153.24	10.40	3.47	935.4	B
	2	2350	1150	2.56	0.34	3,388,620	- 0.37	1762.59	29.47	9.82		
5	1	1728	535	2.12	0.45	605,688	- 0.79	186.87	11.32	3.77	875.9	B
	2	2180	900	2.41	0.40	1,952,083	- 0.59	858.95	21.69	7.23		
6	1	1250	310	1.85	0.47	177,426	- 0.87	37.72	5.72	1.91	573.5	C
	2	3300	750	2.30	0.47	1,295,211	- 0.89	503.23	17.27	5.76		
7	1	1500	460	2.04	0.45	431,179	- 0.79	120.00	9.37	3.12	703	C
	2	2750	780	2.33	0.46	1,414,704	- 0.83	564.57	18.14	6.05		
8	1	1500	530	2.11	0.43	593,026	- 0.71	181.79	11.19	3.73	689.5	C
	2	2900	730	2.29	0.47	1,218,791	- 0.86	464.88	16.70	5.57		
9	1	1375	470	2.05	0.43	452,557	- 0.74	127.81	9.63	3.21	644.5	C
	2	2100	720	2.28	0.43	1,181,546	- 0.73	446.45	16.41	5.47		
10	1	1300	560	2.14	0.39	671,237	- 0.54	213.65	11.99	4.00	783.6	B
	2	2100	760	2.31	0.42	1,334,391	- 0.70	523.16	17.56	5.85		
11	1	1100	260	1.77	0.47	119,438	- 0.88	22.52	4.59	1.53	484.2	C
	2	2650	670	2.24	0.47	1,004,896	- 0.86	361.50	15.00	5.00		
12	1	1567	630	2.20	0.40	874,921	- 0.61	301.79	13.89	4.63	760.5	B
	2	2500	800	2.34	0.44	1,497,632	- 0.77	608.08	18.72	6.24		
13	1	1200	260	1.77	0.48	119,438	- 0.90	22.52	4.59	1.53	450.8	C
	2	2100	630	2.20	0.45	874,921	- 0.80	301.79	13.89	4.63		
14	1	1500	430	2.00	0.46	370,473	- 0.82	98.46	8.62	2.87	760.9	B
	2	3100	810	2.35	0.46	1,540,082	- 0.85	630.64	19.01	6.34		
15	1	1900	300	1.83	0.49	164,807	- 0.95	34.26	5.49	1.83	602	C
	2	2700	730	2.29	0.46	1,218,791	- 0.84	464.88	16.70	5.57		
16	1	1500	370	1.93	0.47	264,184	- 0.87	63.37	7.14	2.38	687.2	C
	21	2700	770	2.32	0.46	1,374,222	- 0.82	543.60	17.85	5.95		
17	1	1750	620	2.20	0.43	843,984	- 0.71	287.96	13.61	4.54	899.1	B
	2	2850	1050	2.50	0.42	2,761,395	- 0.69	1349.87	26.30	8.77		
18	1	1350	610	2.19	0.37	813,663	- 0.49	274.55	13.34	4.45	761.1	B
	2	2000	810	2.35	0.40	1,540,082	- 0.61	630.64	19.01	6.34		
19	1	1500	390	1.96	0.46	297,405	- 0.85	73.95	7.63	2.54	620.9	C
	2	2300	800	2.34	0.43	1,497,632	- 0.72	608.08	18.72	6.24		
20	1	1250	400	1.97	0.44	314,838	- 0.77	79.65	7.87	2.62	762.8	B
	2	2650	950	2.44	0.43	2,204,605	- 0.71	1006.53	23.21	7.74		
21	1	1300	580	2.16	0.38	726,383	- 0.50	236.81	12.52	4.17	762.8	B
	2	2400	860	2.38	0.43	1,762,277	- 0.71	751.74	20.49	6.83		

The projected natural period for each chosen location in the research region is displayed in Table 6. Figure 16 is the map of the natural site period that was created to show that there are three areas, two at the center and the third one in the southwest portion of the research region, where the soils are primarily soft deposits (Table 6), due to the lowest  $V_s^{30}$  values of the alluvium deposits. The locations in the study

area where the soils are composed of soft sediments, such as loose sands, silty clay, and gravels, are much more prone to amplification with higher site periods ranging from 0.199 to 0.27 s.

A number of soil properties, such as the lateral variation, soil type (sand, silt, clay), shear modulus, and damping ratio, have an impact on soil amplification and site natural periods estimation

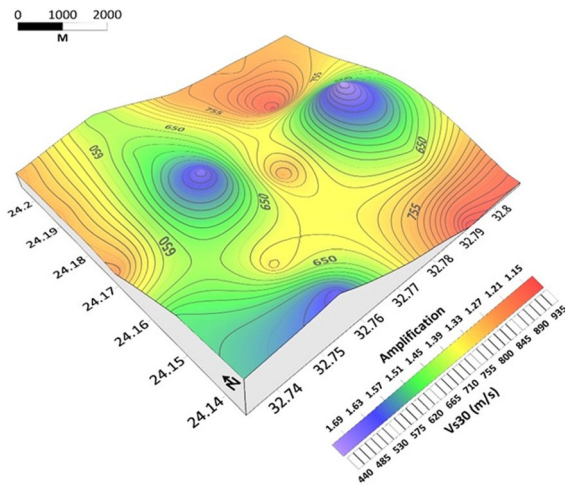


Figure 15

Amplification susceptibility map: amplification values (colored) plotted with  $V_s^{30}$  (solid contour lines) for the study area

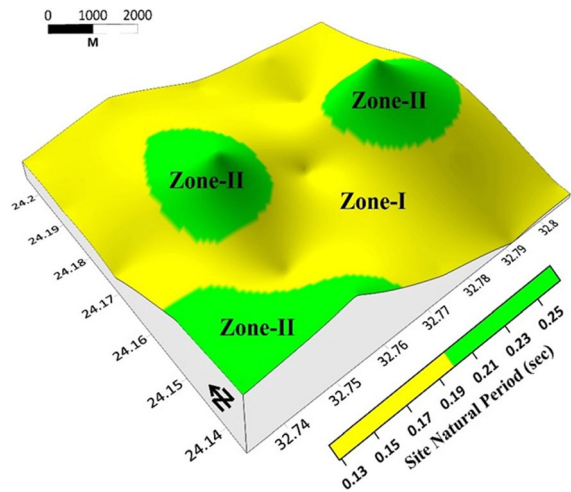


Figure 16

Natural site periods for the study area

(Midorikawa, 1987). Consequently, in this study, the utilized empirical relationships were employed in the current research and only used to calculate the region’s initial soil amplification and resonance frequency from the  $V_s^{30}$  value, since it is the easiest

Table 6

Amplification and site natural period for each point in the study area

P.N	Amplification	Natural site period
1	1.5	0.22
2	1.6	0.24
3	1.3	0.17
4	1.1	0.13
5	1.2	0.14
6	1.5	0.21
7	1.3	0.17
8	1.3	0.17
9	1.4	0.19
10	1.2	0.15
11	1.7	0.25
12	1.3	0.16
13	1.7	0.27
14	1.3	0.16
15	1.5	0.20
16	1.3	0.17
17	1.1	0.13
18	1.3	0.16
19	1.4	0.19
20	1.3	0.16
21	1.3	0.16

and cheapest way to do that. Therefore, the obtained results have to be used as a guide and first step specially for the natural periods of the site because of the importance to avoid the destructive effect of any probable seismic activity that could happen in proximity to the study area (see Fig. 4). Therefore, the Nakamura technique (the Horizontal to Vertical Spectral Ratio method) is recommended for use for microtremor measurements to accurately estimate the value of resonance frequencies, which represent the real and direct measured natural periods for the site, as a result of the impedance contrast between the soil and the underlying bedrock.

#### 5.4. Soil-Structure Interaction (Dynamic Interaction Problem)

The estimated natural period is especially high because of the clay and clayey sand sediments scattered over much of the area and typically has a lower  $V_s^{30}$  value. Because of the greater  $V_s^{30}$  values of the terrace and colluvial sediments, the other sites in the area have natural periods ranging from 0.13 to 0.19 s. The damage to the structures will often be particularly severe if the fundamental site period of the sediments at such places approaches the natural period of the buildings.

The research region was divided into two zones according to their periods since the period estimated

Table 7

Equations for determination of buildings period by ECP-201 (2012) and NEHRP (2003) and height limitations in study area

Standard	Building type	Period equation	Zone-1 (height (m))	Zone-2 (height (m))
NEHRP (2003)	Steel frame	$T = 0.0724h^{0.8}$	1.5–3.3	3–3.6
	Concrete frame	$T = 0.0466h^{0.9}$	2.86–4.76	4–6.75
	Braced	$T = 0.0734h^{0.75}$	1.95–3.5	3–5.4
	Other	$T = 0.0488h^{0.75}$	3.3–6.12	6–9.3
ECP-201 (2012)	Steel frame	$T = 0.08h^{0.75}$	1.7–3.1	3–4.8
	Concrete frame	$T = 0.07h^{0.75}$	2–3.7	3–5.75
	Other	$T = 0.05h^{0.75}$	3.2–5.9	5–9

Table 8

Natural period of building with different stories (Kramer, 1995)

Number of stories	Natural period of the building (T)
1	0.1
2	0.2
3–4	0.3–0.4
5–6	0.5–0.6
10	1.0

Table 9

Classification of buildings based on their height in study area

Standard	Building type	Zone	Stories		
			1 – 3	4 – 10	10 – 15
NEHRP (2003)	Steel frame	1	–	OK	OK
		2	–	OK	OK
	Concrete frame	1	–	OK	OK
		2	–	OK	OK
	Braced	1	–	OK	OK
		2	–	OK	OK
	Other	1	–	OK	OK
		2	–	OK	OK
Ecp-201 (2012)	Steel frame	1	–	OK	OK
		2	–	OK	OK
	Concrete frame	1	–	OK	OK
		2	–	OK	OK
	Other	1	–	OK	OK
		2	–	OK	OK

by the empirical equation will be restricted to 0.12 and 0.27 s, which does not vary significantly. This was done to identify which buildings should be avoided in every zone. The first zone's periods range

from 0.12 to 0.19 s, and the second zone's periods range from 0.19 to 0.27 s (Fig. 16).

Indeed, calculating the seismic loads according to design codes like NEHRP (2003), EC8, ASCE7-10, UBC 97, and ECP-201 (2012) necessitates estimating the building's fundamental period. The basic period could be calculated using a variety of techniques. To predict the period of the buildings, however, design regulations advise using simplified empirical formulas as a preliminary stage. The kind and height of buildings that should be avoided in these two districts are identified using the techniques proposed by ECP-201 (2012) and NEHRP (2003). Table 7 lists the calculations in the cited codes as well as the building height restrictions of each zone. In particular, the severity of the destruction to the buildings increases as the fundamental frequency (natural period) of the strata matches that of the building.

In principle, it is necessary to accept a defined period within every zone for the construction of safe buildings if somehow the buildings are divided into three categories of 1–3, 4–10, and 10–15 story buildings (typical building height in Egypt). Due to the exactly equal values of the periods among both buildings and soil, Table 8 demonstrates that one- to two-story buildings are much more particularly prone to seismic risk in the majority of the study region; in addition, one- to three-story buildings are more susceptible to damage in three other areas in the study region.

Consequently, the soil characteristics of New Aswan City's western extension frequently provide a possible risk of damage, particularly to one- to three-story structures during an earthquake. Table 9 lists the applicable requirements for structures based on



ECP 201 (2012) and NEHRP (2003). There would be no restrictions for such buildings if their period did not fall between 0.12 and 0.19s in zone 1 and between 0.19 and 0.27s in zone 2; therefore, Table 9 presents them correctly.

## 6. Discussion

Generally, the study area is composed of two layers, according to the lithologic cross-section (Fig. 2), and the seismic cross-sections of the surface/subsurface strata that are obtained from the shallow seismic refraction data. The surface layer has  $V_p$  927–1900 m/s and shear wave velocities ( $V_s$ ) around 260–630 m/s to a depth of approximately 5 m. The second layer extends from 5 to 20 m depth; it has  $V_s$  range values between 520 and 1150 m/s and corresponding  $V_p$  values between 2000 and 3300 m/s. The higher compressional and shear wave velocity values could be related to the consolidated sandstone mainly occurring in the study area.

Since bedrock site frequently produces lower ground-motion intensities than less rigid places, the geotechnical engineering properties are critical for any future infrastructure development project. The elastic properties of rocks that are close to the Earth's surface including their impact on wave propagation are critical in seismic design. To determine whether subsurface materials are acceptable for construction, some selected geotechnical parameters have been chosen to be estimated for the purpose. As a result, estimations were made for the soil's dynamic characteristics, including density, Poisson's ratio, rigidity modulus, Young's modulus, bulk modulus, allowable maximum bearing capacity, and ultimate bearing capacity. Those factors, which depended on  $V_s$  and  $V_p$ , are acquired through compressional waves created using shallow seismic refraction's 2D profiles and from 1D- $V_s$  models generated from the MASW approach. For instance, it has been calculated that the first- and second layer's densities vary between 1.8 and 2.2 g/cm<sup>3</sup> and 2.1 and 2.6 g/cm<sup>3</sup>, respectively. A significant increase in calculated values is an

indication of a rather high competent rock composition that characterizes the second stratum.

The generated  $V_s$  models were used to calculate the  $V_s^{30}$ . Utilizing the NEHRP site classification for earthquake resistance design, it can be shown that the  $V_s^{30}$  values almost fall between 450 and 935 m/s. Consequently, the area is split into two groups, in accordance with NEHRP standards: The western edge of the investigated region has Class B (Rock) sites (North-East, South-East) and central parts; however, Class C makes up the rest of the research area and is distinguished by incredibly thick soil with soft rock. In addition, the soil amplification map derived from MASW technique displays values between 1.1 and 1.7, with high amplification in the same three zones which existed in  $V_s^{30}$  map. Additionally, according to the produced site natural period map, the three zones mentioned above, in which the soils are composed of soft sediments (such as loose sands, and gravels), are more prone to amplification with significantly higher site periods. However, the natural periods at the other sites in the city are lower. So, we could say, the research area is separated into two zones according to the calculated natural periods. If the structures are divided into three categories of 1–3, 4–10, and 10–15 story buildings based on the typical construction heightening in Egypt, one- to three-story structures seem to be more susceptible to earthquakes in most of the study region since the periods between the structure and the soil are identical in value.

In general, the higher values of soil amplification and natural periods have mostly been interpreted based on the sediment content of the soft alluvial plain as well as some river terraces. Accordingly, places with soft sediments, such as unconsolidated Quaternary deposits, are much more vulnerable to amplification. The geologic features observed in the field work and deduced from the scientific literature indicate that the moderate to compacted sandstone which may intercalate with shale is dominant and plays an essential role in the geotechnical parameter's high values, with exception of the three previously

mentioned zones, which may suffer from higher soil amplification.

### 7. Conclusion

In the western extension of New Aswan City, we conducted 21 pairs of profiles of shallow seismic refraction and MASW to measure the compressional and shear wave velocity. The sedimentary rocks in the study area are distinguished into two layers, the first of which could be made up of loose sand and clay, while the second layer represents the bedrock, which has relatively high values of both  $V_p$  and  $V_s$ . Based on these geophysical characteristics and geologic evidence, we have deduced that the foundation layer is made up of compacted strata of sandstone. Additionally, the geotechnical parameters have been estimated for site effect evaluation. The NEHRP classification system has been applied, which reveals that the majority of the study area is classified as type C. Empirical equations have also been used to obtain the site amplification factor and the soil's natural period. We could conclude that the geologic features and compactness level of the rocks in the study area play an essential role in the compressional, shear wave, geotechnical parameter, amplification and site natural period values. All of these obtained geophysical criteria will help in establishing the suitable and safe design for the study area.

### 8. Recommendations

Due to the limitations of financial support, we could state that the data collected provide a broad perspective of the geotechnical features for the research region. A condensed study must be conducted to track any potential minor lateral variations in the soil's characteristics. In addition, we recommend using other geophysical tools such as the Nakamura technique to assess the accurate natural period for the site.

### Acknowledgements

The National Research Institute of Astronomy and Geophysics provided financial support for the authors to complete this work, for which they are extremely thankful. We also express our gratitude to the workers of the Aswan Regional Earthquake Research Center for their assistance in data collection. Our gratitude extends to the Editor of the Pure and Applied Geophysics Journal and to the unknown reviewers for their valuable comments which improved the final shape of the research.

**Author Contributions** All researchers were involved in the conceptualization and design of the study. AMM, AH, MK, MEB, EG and AT were in charge of the preparation of the material and the data collecting. However, AH and MK were responsible for the data analysis and first draft of the paper, and all researchers offered feedback on earlier drafts. The final draft was read by all authors before its approval.

### Funding

The National Research Institute of Astronomy and Geophysics (NRIAG) in Cairo, Egypt, has financed this study.

### Data Availability

The data that support the findings of this study are available on request from the corresponding author.

### Declarations

**Conflict of interest** The authors do not have any material financial or non-financial interests to disclose. However, the financing was solely provided by our institute, NRIAG, in Cairo, Egypt.

**Publisher's Note** Springer Nature remains neutral with regard to jurisdictional claims in published maps and institutional affiliations.

Springer Nature or its licensor (e.g. a society or other partner) holds exclusive rights to this article under a publishing agreement with the author(s) or other rightsholder(s); author self-archiving of the accepted manuscript version of this article is solely governed

by the terms of such publishing agreement and applicable law.

#### REFERENCES

- Abbas, M.A., Fat-Helbary, R.E.-S., Hamed, A., El-Faragawy, K.O., El-Amin, E.M., El-Qady, G.M. (2023). The implementation of shallow geophysical survey for detection of some buried archaeological structures in Aswan City, Egypt. In: *Sustainable conservation of UNESCO and other heritage sites through proactive geosciences*. Springer Geology. [https://doi.org/10.1007/978-3-031-13810-2\\_11](https://doi.org/10.1007/978-3-031-13810-2_11).
- Abd El-Rahman, M. (1989). Evaluation of the kinetic elastic moduli of the surface materials and application to engineering geologic maps at Maba-Risabah area (Dhamar Province), Northern Yemen, Egypt. *Journal of Geology*, 33, 229–250.
- Abd El Rahman, M., Setto, I., & El-Werr, A. (1992). Inferring mechanical properties of the foundation materials at the 2nd Industrial zone. In *10th of Ramadan City, from geophysical measurements. E.G.S. Proceedings of the 10th anniversary meeting* (pp. 50–61).
- Abudeif, A., Raef, A., Moneim, A. A., Mohammed, M., & Farrag, A. (2017). Dynamic geotechnical properties evaluation of a candidate nuclear power plant site (NPP): P-and S-waves seismic refraction technique, North Western Coast, Egypt. *Soil Dynamics and Earthquake Engineering*, 99, 124–136.
- Attia M. I. (1955). *Topography, geology and iron ore deposits of East Aswan: Geological Survey*, Egypt, Cairo, Internal Report.
- Birch, F. (1966). Handbook of physical constants. Geological Society of America Membrane, 96, 613.
- Boore, D. M. (2003). Simulation of ground motion using the stochastic method. *Pure and Applied Geophysics*, 160, 635–675.
- Boore, D. M., Thompson, E., & Cadet, H. (2011). Regional correlations of VS30 and velocities averaged over depths less than and greater than 30 meters. *Bulletin of the Seismological Society of America*, 101, 3046–3059.
- Borcherdt, R. D. (1994). Estimates of site-dependent response spectra for design (methodology and justification). *Earthquake Spectra*, 10(4), 617–653.
- Bowles, J. E. (1984). *Geotechnical and physical properties of soil* (2nd ed.) (pp. 32–40).
- CEN. (2004). *Eurocode 8: Design of structures for earthquake resistance-Part 1: General rules, seismic actions and rules for buildings (EN 1998-1: 2004)*. European Committee for Normalization.
- CONOCO. (1987). Geological map of Egypt, Scale 1:500000. The Egyptian General Petroleum Corporation. Conoco Coral.
- De Beer, M., & Maina, J. (2008). Some fundamental definitions of the elastic parameters for homogeneous isotropic linear elastic materials in pavement design and analysis. In *Proceedings of the 27th Southern African transport conference* (pp. 282–293). Document Transformation Technologies.
- Dobry, R., Borcherdt, R., Crouse, C., Idriss, I., Joyner, W., Martin, G. R., Power, M., Rinne, E., & Seed, R. (2000). New site coefficients and site classification system used in recent building seismic code provisions. *Earthquake Spectra*, 16, 41–67.
- Dutta, N. P. (1984). Seismic refraction method to study the foundation rock of a dam. *Journal of Geophysical Prospecting*, 32, 1103–1110. <https://doi.org/10.1111/j.1365-478.1984.tb00757.x>
- Egyptian Geological Survey and Mining Authority. (2002). *A geological map of Assiut Area, scale 1:100,000*.
- Egyptian Loading Code, ECP-201. (2012). pp. 108–158.
- El Bastawesy, M., Faid, A., & Gammal, E. S. E. (2010). The Quaternary development of tributary channels to the Nile River at Kom Ombo area, Eastern Desert of Egypt, and their implication for groundwater resources. *Hydrological Processes*, 24(13), 1856–1865.
- El-Bohoty, M., Ghamry, E., Hamed A., Khalifa, M., Taha, A., & Meneisy, A. (2023). Surface and subsurface structural mapping for delineating the active emergency spillway fault, Aswan, Egypt, using integrated geophysical data. *Journal Acta Geophysica*. <https://doi.org/10.1007/s11600-023-01133-1>.
- El-Khashab, H. M. A., Hassib, G. H., Ibrahim, E. M., & Dessoky, M. M. (1991). Seismicity and composite focal mechanism for microearthquakes in Kalabsha area west of Aswan Lake and their tectonic implication. *Journal of Geodynamics*, 14, 87–104.
- El-Moghazy, M. (2017). *Geotechnical studies using geophysical techniques on North Eastern Al-Fayum city, Egypt* (p. 135). Master thesis. Geophysics Department, Faculty of Science, Al-Azhar University, Egypt.
- Ellefsen, K. J. (2009). A comparison of phase inversion and travel time tomography for processing near-surface refraction travel times. *Geophysics*, 74(6), WCB11–WCB24.
- Fat-Helbary, R. E., El-Faragawy, K. O., & Abdel Motaal, A. M. (2004). Land use planning and seismic hazards of the proposed Aswan New City area, Egypt. *Acta Geodynamica Et Geomaterialia*, 1(4), 99–106.
- Fat-Helbary, R. E., El-Faragawy, K. O., & Abdel Motaal, A. M. (2006). Engineering seismological studies on the proposed location of Aswan New City, Egypt. *Acta Geodaetica Et Geophysica Hungarica*, 41(2), 211–225. <https://doi.org/10.1556/AGeod.41.2006.2.6>
- Fat-Helbary, R. E., El-Faragawy, K. O., & Hamed, A. (2019a). Application of HVSR technique in the site effects estimation at the South of Marsa Alam City, Egypt. *Journal of African Earth Sciences*, 154, 89–100. <https://doi.org/10.1016/j.jafrearsci.2019.03.015>
- Fat-Helbary, R. E. S., El-Faragawy, K. O., & Hamed, A. (2019b). Soil geotechnical characteristics for seismic risk mitigation at the southern extension of Marsa Alam city, Egypt. *NRIAG Journal of Astronomy and Geophysics*, 8(1), 1–14.
- Gardner, G. H. F., Gardner, L. W., & Gregory, A. R. (1974). Formation velocity and density—The diagnostic basics for stratigraphic traps. *Geophysics*, 39, 770–780.
- Grit, M., & Kanli, A. I. (2016). Integrated seismic survey for detecting landslide effects on high speed rail line at Istanbul-Turkey. *Open Geosciences*, 8(1), 161–173.
- Hamed, A. (2019). *Seismic microzonation for earthquake risk mitigation at the southern extension of Marsa Alam City*. Ph.D.'s Thesis. Aswan University, Aswan, Egypt.
- Hamed, A., Fat-Helbary, R. E., Mohamed E., M., and El-Faragawy, K. O. (2023). Seismic site characteristics for geotechnical engineering purposes: Case study, South of Ras Samadai, Red Sea, Egypt. *Journal of Applications Geophysical*. <https://doi.org/10.1016/j.jappgeo.2023.105223>.

- Hodgkinson, J., & Brown, R. J. (2005). Refraction across an angular unconformity between nonparallel TI media. *Geophysics*, 70(2), D19–D28.
- Imai, T., & Yoshimura, Y. (1975). The relation of mechanical properties of soils to P and S-wave velocities for ground in Japan Technical Note OYO Corporation. In *4th Japan earthquake engineering symposium* (pp. 89–96).
- Issawi, B. (1968). The geology of Kurkur Dungul area: Cairo, General Egyptian 767 Organization for Geological Research and Mining, Geological Survey, no. 46, 102p.
- Issawi, B., Francis, M., Youssef, A., & Osman, R. (2009a). *The Phanerozoic of Egypt: A geodynamic approach*. Egyptian Geological Survey, Special Publication 81.
- Issawi, B., Francis, M., Youssef, A., & Osman, R. (2009b). The phanerozoic of Egypt: A geodynamic approach. *Geological Survey Egypt Special Publication*, 81, 589.
- Kanai, K. (1952). Relation between the nature of surface layer and amplitudes of earthquake motions. Part I–IV. *Bulletin of Earthquake Research Institute Tokyo University (i)*, 30, 31–37.
- Kanli, A. I. (2010). Integrated approach for surface wave analysis from near-surface to bedrock, Chap. 29, pp. 461–476, *Advances in near-surface seismology and ground-penetrating radar, geophysical developments series no. 15*, SEG Reference Publications, Society of Exploration Geophysics Reference Publications Program, Tulsa, Oklahoma-USA. Society of Exploration Geophysicists, American Geophysical Union and Environmental and Engineering Geophysical Society (Ed. Com.: R.D. Miller, J.D. Bradford and K. Holliger), ISBN 978-0-931830-41-9 (Series); ISBN 978-1-56080-224-2 (Volume).
- Kanli, A. I., Kang, T. S., Pinar, A., Tildy, P., & Pronay, Z. (2008). A systematic geophysical approach for site response of the Dinar Region, South Western Turkey. *Journal of Earthquake Engineering*, 12(S2), 165–174.
- Kanli, A. I., Tildy, P., Pronay, Z., Pinar, A., & Hermann, L. (2006). VS30 mapping and soil classification for seismic site effect evaluation in Dinar Region, SW Turkey. *Geophysical Journal International*, 165(1), 223–235.
- Kearey, P., Brooks, M., & Hill, I. (2002). *An introduction to geophysical exploration* (pp. 1–20). Blackwell.
- Kebeasy, R. M., Maamoun, M. M., Ibrahim, E. M., Megahed, A., Simpson, D. W., & Leith, W. L. (1987). Earthquake studies at Aswan reservoir. *Journal of Geodynamics*, 7, 173–193.
- Keceli, A. D. (2009). *Applied geophysics, UCTEA chamber of geophysical engineers, Ankara, Turkey, July 2009*. <http://jeofizik.org.tr> (in Turkish).
- Kramer, S. L. (1995). *Geotechnical earthquake engineering*. Prentice Hall.
- Lankston, R. W. (1989). The seismic refraction method: A viable tool for mapping shallow targets into the 1990s. *Geophysics*, 54(12), 1535–1542.
- Luna, R., & Jadi, H. (2000). Determination of dynamic soil properties using geophysical methods. In *Proceedings of the first international conference on the application of geophysical and ndt methodologies to transportation facilities and infrastructure, St. Louis, MO* (pp. 1–15).
- Meneisy, A. M., Toni, M., & Omran, A. A. (2020). Soft sediment characterization using seismic techniques at Beni Suef City, Egypt. *Journal of Environmental and Engineering Geophysics*, 25, 391. <https://doi.org/10.32389/JEEG19-06>
- Midorikawa, S. (1987). Prediction of isoseismal map in the Kanto plain due to hypothetical earthquake. *Journal of the Structural Engineering*, 33B, 43–48.
- Miller, R. D., Xia, J., Park, C. B., & Ivanov, J. M. (1999). Multichannel analysis of surface waves to map bedrock. *The Leading Edge*, 18(12), 1392–1396.
- Mohammed, M. A., Abudeif, A. M., & Abd El-aal, A. K. (2020). Engineering geotechnical evaluation of soil for foundation purposes using shallow seismic refraction and MASW in 15th Mayo, Egypt. *Journal of African Earth Sciences*, 162, 103721.
- Mohammed, M. A., Abudeif, A. M., Omar, K. A., & Attia, M. M. (2018). Estimation of site effect using microtremor technique at 15th May City, Helwan, Egypt. *Arabian Journal Geoscience*, 11, 16.
- NEHRP. (2003). Recommended provisions for seismic regulations for new buildings and other structures. In *Building Seismic Safety Council (BSSC) for the Federal Emergency Management Agency (FEMA 450)*. FEMA, Washington Part 1: Provisions.
- Ooba, S. (1957). Study of the relation between subsoil conditions and the distribution of damage percentage of wooden dwelling houses in the province of Totomi in the case of the Tonankai Earthquake of December, 7th, 1994. *Tokyo University Earthquakes Research Institute Bulletin*, 36, 201–295.
- Park, C. B., Miller, R. D., & Xia, J. (1998). *Imaging dispersion curves of surface waves on multi-channel record: Technical Program with biographies*, SEG, 68th Annual Meeting, New Orleans, Louisiana, pp. 1377–1380.
- Park, C. B., Miller, R. D., & Xia, J. (1999). Multichannel analysis of surface waves. *Geophysics*, 64(3), 800–808.
- Parry, R. H. (1977). Estimating bearing capacity of sand from SPT values. *JGED ASCE*, 103, 1014–1043.
- SeisImager. (2009). *SeisImager/2DTM Manual Version 3.3*.
- SeisImager. (2019). *Windows software package for seismic refraction analysis, Ver. 5*. Geometrics Inc.
- Sharma, P.V. 1978. *Geophysical Methods in Geology*, Second ed. Elsevier, Oxford, New York.
- Sheehan, J. R., Doll, W. E., & Mandell, W. (2005). An evaluation of methods and available software for seismic refraction tomography analysis. *Journal of Environmental and Engineering Geophysics*, 10(1), 21–34.
- Sheriff, R. E., & Geldart, L. P. (1995). *Exploration seismology*. Cambridge University Press.
- Simpson, D. W., Kebeasy, R. M., Nicholson, C., Maamoun, M., Albert, R. N., Ibrahim, E. M., Megahed, A., Gharib, A., & Hussain, A. (1986). Aswan telemetered seismograph network. *Journal of Geodynamics*, 7, 195–203.
- Stokoe, K. H., II., Wright, G. W., Bay, J. A., & Roesset, J. M. (1994). Characterization of geotechnical sites by SASW method. In R. D. Woods (Ed.), *Geophysical characterization of sites*. Oxford Publishers.
- Stümpel, H., Kähler, S., Meissner, R., & Milkereit, B. (1984). The use of seismic shear waves and compressional waves for lithological problems of shallow sediments. *Geophysical Prospecting*, 32(4), 662–675.
- Tatham, R.H. (1982). Vp/Vs and lithology. *Geophysics*, 47(3), 336–344.
- Telford, W.M., Geldart, L.P., Sheriff, R.E., and Keys, D.A., 1976. *Applied Geophysics*. Cambridge University Press, Cambridge.
- Underwood, D. (2007). *Near-surface seismic refraction surveying field methods*. Geometrics Inc.

- Veezhinathan, J., & Wagner, D. (1990). A neural network approach to first break picking. In *IJCNN international joint conference on neural networks* (Vol. 1, pp. 235–240). IEEE, New York, NY.
- Whiteley, R. J. (1994). Seismic refraction testing—A tutorial. In R. D. Woods (Ed.), *Geophysical characterization of sites* (pp. 45–47). Oxford & IBH Publishing.
- Woodward-Clyde Consultants. (1985). *Earthquake activity and Dam stability valuation for the Aswan High Dam, Egypt, Five volumes*.
- Xia, J., Miller, R. D., Park, C. B., Hunter, J. A., & Harris, J. B. (2000). Comparing shear-wave velocity profiles from MASW with borehole measurements in unconsolidated sediments, Fraser River Delta, BC, Canada. *Journal of Environmental & Engineering Geophysics*, 5(3), 1–13.
- Yilmaz, O., Eser, M., & Berilgen, M. (2006). Seismic, geotechnical, and earthquake engineering site characterization. In *SEG technical program expanded abstracts 2006* (pp. 1401–1405). Society of Exploration Geophysicists.
- Yousif, M. (2019). Hydrogeological inferences from remote sensing data and geoinformatic applications to assess the groundwater conditions. El-Kubbaniya basin, Western Desert, Egypt. *Journal of African Earth Sciences*, 152, 197–214.
- Youssef, M. M. (2003). Structural setting of central and south Egypt: An overview. *Micropaleontology*, 49(Suppl\_1), 1–13.

(Received September 4, 2022, revised July 14, 2023, accepted October 20, 2023, Published online November 12, 2023)